IADC/SPE-212560-MS

Performance Analysis of a Downhole Regulator on Rate-Of-Penetration and Drilling Efficiency: An Autonomous Load Management at Bit

Arviandy G. Aribowo, Eindhoven University of Technology; Ulf Jakob F. Aarsnes, Norwegian Research Centre, NORCE AS; Emmanuel Detournay, University of Minnesota; Nathan Van de Wouw, Eindhoven University of Technology; Nils Reimers, Tomax AS

This paper was prepared for presentation at the IADC/SPE International Drilling Conference and Exhibition, Stavanger, Norway, 7 – 9 March 2023.

Abstract

Over the last years, the use of autonomous solutions for balancing the loading on the drill-bit has increased annually. By 2021, downhole tools for this purpose have been used for more than 1,500 wells and these become possibly the fastest growing trend in drilling. Polycrystaline Diamond Compact (PDC) drill-bits represent a great potential for drilling economics when steady cutting is attainable. Deep drilling, however, typically involves long drillstring causing an array of dynamic instabilities preventing steady cutting conditions at the bit. Such behavior affects drilling performance in terms of the rate-of-penetration (ROP) and system damage and failure. This leaves a big potential for improvement of drilling performance. The first experiments with an autonomous downhole regulator constructed were completed at Ulrigg in Stavanger almost twenty years ago to tap into this potential. Several versions of similar tools have since developed using a variety of mechanical and hydraulic functions to modify and shift the forces acting on the drill-bit in order to improve drilling performance.

The Norwegian operator Equinor has participated from the very start of this new automation trend. By 2020 they had deployed downhole regulators to a total of 93 well sections on the Norwegian Continental Shelf alone. In this paper, Equinor shares statistic plots from comparing these first 93 sections to well section with conventional BHA's. The data show how the continuous improvement of the regulator eventually led to gradual improvement of both ROP and footage - in addition to its initial task of reducing vibrations. By utilizing a variety of dynamic models, predictions and sensitivity analysis, it has been revealed that the downhole regulator could change the dynamic response of the bit such that the friction losses at the bit are reduced and the rock cutting efficiency is improved. In this paper, it is shown that such benefits can also be expected in real-life scenarios in which two key aspects play a role: 1) a PDC bit penetrating heterogeneous layers of rock formations, and 2) involving two frictional losses due to borehole - drillstring contact in deviated wells.

This paper brings a unique insight to the fundamentals, advanced mathematical models, and statistical results from a new line of drilling technology. The autonomous regulators bring a combination of reduction in risk and time to drill that makes a significant impact on cost.

Introduction

The modern fixed-cutter polycrystalline-diamond-compact (PDC) drill-bit technology has shown high efficiency in rock cutting process; however, its interaction with the rock formation also has a proven potential for producing dynamic forces and energy shocks with significant destructive levels to the bit itself, the instrumented BHA, and the drillstring connections (Fear *et al.*, 1997). Hence as a solution, a downhole autonomous load management system (or simply called as downhole regulator (DR)) is designed with an aim of managing the dynamical loading acting on the drill-bit (for preventing premature failure caused by these high energy shocks). The design of this DR is focused on autonomously stabilizing the forces acting on the drill-bit, particularly to effect a change in the axial loading proportional to the change in torsion suitable for a PDC bit.

The first testing of a prototype of such DR took place in 2005 at the Ulrigg test facility in Stavanger. The two Norwegian operators (Statoil and Norsk Hydro) supported the testing program; these same companies later merged and became what is known today as Equinor. In this test, the recorded results on the positive influence of the regulator have shown a significant reduction in symptoms of drillstring overload and a measurable improvement in drilling performance (ROP) – as presented and reported in (Selnes *et al.*, 2008, 2009). Together with BP, these three companies implemented this invention of DR in the field. Moreover, the field results obtained with the new downhole regulator have attracted the attention of academia, including some of the co-authors to this paper from the Eindhoven University of Technology in the Netherlands, the University of Minnesota in the USA, and the Norwegian Research Centre. These research groups had extensively published their research results in the field of dynamical control systems and deep drilling.

Their earlier works presented in (Vromen *et al.*, 2019; Vromen, 2015) have contributed in the development of modelling and dynamic analysis of drilling systems equipped with a downhole regulator for a vertical wellbore with homogeneous rock properties. These works have analyzed the effect of the DR installed in the bottom-hole-assembly (BHA) on drilling performance in terms of rate-of-penetration (ROP) and drilling efficiency (mechanical specific energy (MSE)).

In particular, this DR is represented by a dynamic structural model that consists of an internal preloaded spring, a structural damper, and a helical spline which couples the axial and torsional dynamics of the drillstring system. In addition, the bit-rock interface laws in (Detournay & Defourny, 1992; Detournay *et al.*, 2008) are applied as the bottom boundary conditions of the drillstring model that contribute to the axial and torsional dynamics in terms of weight-on-bit (WOB) and torque-on-bit (TOB) due to the cutting process and (frictional) contact in the bit-rock interaction.

As the contributions of this paper, first we present some field results of the DR implementation. Equinor has generously shared relevant drilling records that cover the full DR field implementation period for this paper. The records have thousands of well sections with a large variety of deviations and hole sizes. Figure 1 shows a map of the Norwegian Continental Self (NCS) with the location of the fields where the regulator has been in use and where performance data have been compared. Only fields with well clusters and thus more than a minimum of five reference sections are part of the study. An example of a well cluster accepted for comparisons is the Gullfaks platforms shown in Figure 2.

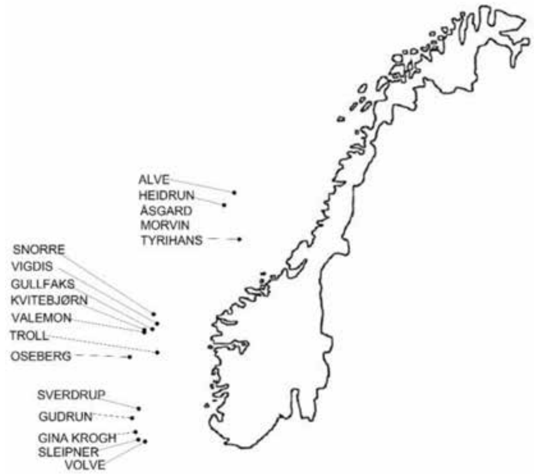

Figure 1—The new downhole regulator has been used in different well sections in the fields named on this map.

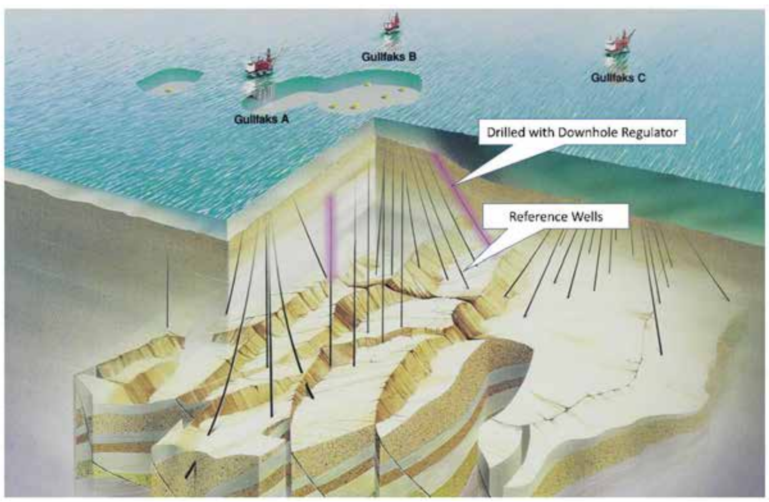

Figure 2—The offshore fields, such as Gullfaks, have many parallel trajectories and form a good case for performance comparison in several sections of the wells.

Second, we summarize the latest extension of this modelling work to study the effect of the same DR on drilling performance under other real drilling circumstances, such as 1) the drilling of deviated wellbores, and 2) the drilling in interbedded formations. In addition, we summarize the simulation results for each of drilling scenario and perform qualitative comparisons between the simulation results (theoretical, model-based) and the field implementation results of a DR (field-based), in order to check the consistency on the effect of such DR on drilling performance.

This paper is organized as follows. Section 2 presents the field data from the Equinor that show the effect of such downhole regulator on drilling performance. In Section 3, we summarize the frameworks of dynamic modelling extension for drilling systems equipped with the downhole regulator in two separated drilling scenarios, namely 1) in deviated wellbore trajectory, and 2) in interbedded formations. In Section 4, the summary of the dynamic analysis, based on the simulation results for each drilling scenario, is presented. In this analysis, we qualitatively verify the consistency of the simulation results with the field results. Finally, conclusions are drawn in Section 5.

Field results observations: Statistical field data of the regulator effect

Equinor has used the DR technology since 2006. A total number of 93 sections from this period have been selected for this study based on several criteria. The main criterion is to exclude the sections where the bit was pulled off for any other reason than completed drilling or poor progress. Our goal is to obtain a simple but reliable statistical reference that reflects the actual DR performance for qualitative comparison to the theoretical model simulations.

The Equinor statistical data in this paper show the effect of the regulator on drilling efficiency and reducing the friction losses at the bit-rock interface (which can also be associated to bit wear). This effect can be assessed via the comparisons of ROP and of footage, meaning drilled distance per bit. If the friction is successfully reduced with the application of DR, the ROP will simultaneously increase (as more energy is directed the cutting process at the bit), and this is also accompanied by reduced bit wear.

In the purpose of displaying this unique relationship of improved ROP and increased drill-bit durability, the data from a number of well sections drilled without any regulator in a given field are averaged and compared to the relevant data from similar sections drilled with the DR tool in the same field. The differences or changes (in percentages) per field are then showed as bubbles plots in a 2D plot; Each bubble represents an oilfield or a platform, where we compare the averaged data with and without the application of DR. The ROP improvement per field runs along the horizontal axis, i.e., indicating how much ROP is improved on this oilfield or platform by including the DR in the BHA. Similarly, the reduction in wear resulting in footage gains from the comparisons in the same field are on the vertical axis. The radial sizes of the bubbles give the number of sections that have used a regulator in drilling that field, i.e., a larger radius shows more runs with the DR in the part of the comparison on this platform or oilfield.

In summary, the statistics in Figure 3 and Figure 4 show the positive effect of the DR application in terms of ROP improvement and footage gains on average, i.e., more positive percentage values on the ROP and footage changes. Figure 3 shows the comparison plot covering the first dataset obtained before 2015 using a regulator with a limited operational range. Figure 4 shows the sections drilled after 2015 using the current regulator with a full operational range. Note also that if a bubble is having a negative percentage value (either for ROP changes or footage gains), this means that in that particular field (or platform) the use of the regulator did not bring improvement on the performance and there might be any additional operational issue causing slower drilling or less footage on average.

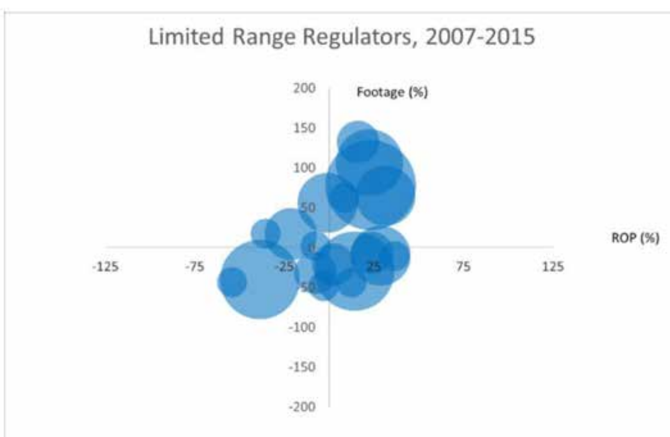

Figure 3—The plot illustrates the differentiation in performance for ROP and Footage for a drillstring with the first downhole regulators versus a standard system in the same field and well sections.

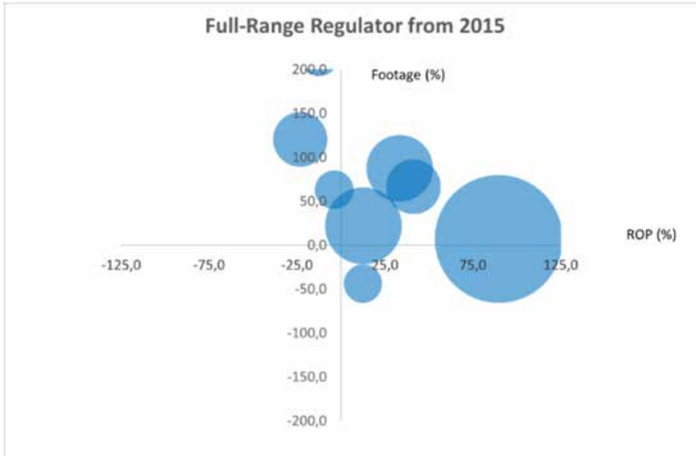

Figure 4—The plot illustrates the differentiation in performance for ROP and Footage for a drillstring with the current downhole regulator versus a standard system in the same field and well sections.

Nevertheless, the introduction of the current DR technology was aimed at expanding the operational range of the regulator. As a result, the ROP improvement and footage gains are obtained in much higher percentages (on average) in Figure 4 - as qualitatively compared with the statistics in Figure 3, i.e., blue circles located in the first quadrant of the plane. It must also be noted that the regulator is listed by Equinor as Best-Practice in more areas than ROP and footage. These areas are challenging rocks, tough under-reaming and rig heave; see for example (Beeh *et al.*, 2018).

Dynamic modelling including the downhole regulator

In this section, we summarize the extensions of the dynamic models of a drillstring system equipped with a downhole regulator (DR) for three drilling scenarios. We refer to the model developed earlier in (T. Vromen *et al.*, 2019) as the basis of the extension.

Firstly, we summarize the extended dynamic model for drilling scenario in a deviated wellbore based on (Wildemans *et al.*, 2019). Secondly, the extended dynamic model for drilling scenario in interbedded formations based on (Aribowo *et al.*, 2022b, 2022a) is presented. All these models are used to study and analyze the effect of the downhole regulator on drilling performance in terms of rate-of-penetration (ROP) and drilling efficiency under the influence of these two drilling scenarios, separately. Furthermore, only the axial and torsional dynamics of the drilling system are considered in this paper.

Dynamic model of drilling system with downhole regulator (DR) in deviated wells

Figure 5 shows the schematic of drilling system in a deviated wellbore with the regulator located in between two stabilizers in the BHA. A lumped-parameter model as depicted in Figure 6 is used to derive the equations of motion (EOMs) of the drillstring dynamics involving the contacts between the stabilizers and borehole wall (in the form of spatial Coulomb friction; see the red lines in the left side) due to the deviated wellbore.

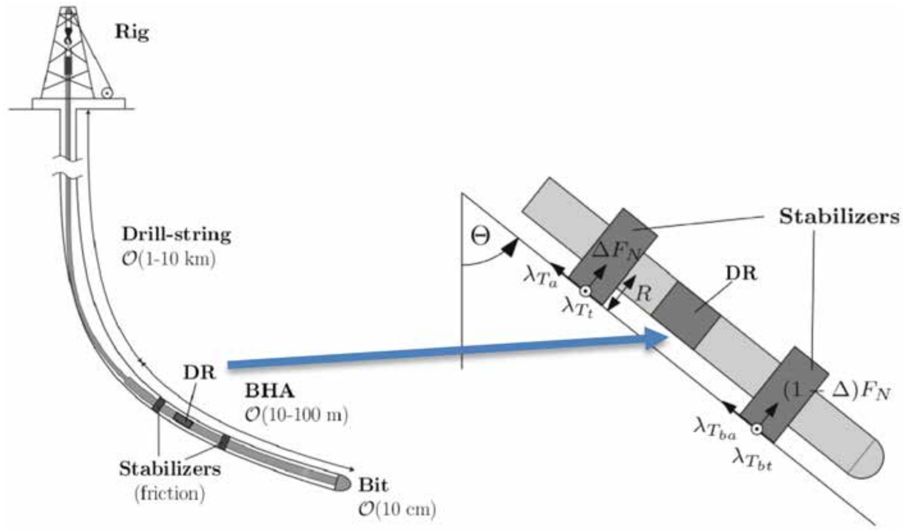

Figure 5—Schematic overview of drilling system with downhole regulator (DR) in a deviated well – see (Wildemans et al., 2019).

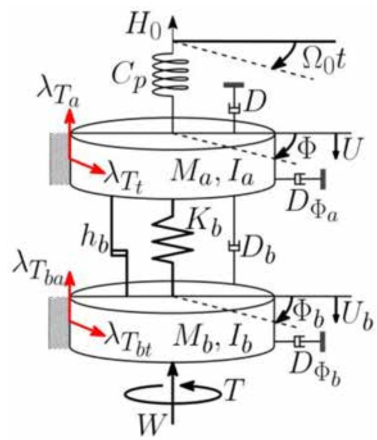

Figure 6—Lumped-parameter model of drillstring system equipped with the DR and affected by the spatial friction due to the contact between borehole and stabilizers – see (Wildemans et al., 2019).

This spatial friction is considered to mainly act on the stabilizers due to its larger diameter as part of the BHA. According to the torque and drag models in (Johancsik *et al.*, 1984; Sheppard *et al.*, 1987), this friction is determined by the normal force and the friction coefficient between the contact surfaces. Moreover, this normal force (denoted by F_N) is affected by the buoyed weight of the drillstring (gravitational effect) and the inclination angle Θ of wellbore as illustrated in Figure 5. A distribution parameter Δ is considered to enable the cases of whether all the spatial friction acts only above or below the regulator. In this modeling, the effect of the tension acting through the curvature of the borehole on the normal force is omitted.

The bit-rock interface laws developed in (Detournay & Defourny, 1992; Detournay *et al.*, 2008) are applied as the bottom boundary conditions and mainly composed by the bit-rock parameters for the cutting and frictional components (in both axial and torsional directions) of this bit-rock interaction.

The EOMs of the axial and torsional dynamics of this drilling system are written in the following form:

$$\mathbf{M}\ddot{\mathbf{q}} - \mathbf{h}(t, \mathbf{q}, \dot{\mathbf{q}}) = \mathbf{W}_{\lambda}\boldsymbol{\lambda}, \tag{1}$$

where $\mathbf{M}$ is the mass matrix and the column vector $\mathbf{q}$ represents the generalized coordinates describing the drillstring response. The column vector $\mathbf{h}$ contains all generalized (smooth) forces and torques, which excludes the contact forces and the frictional torques acting on the bit and the frictional forces and torques acting on the stabilizers (all modelled by non-smooth force laws - see (Leine & van de Wouw, 2008)).

The smooth forces and torques are contributed by the structural damping (axial damping above and of the regulator: with damping coefficients D and D_b, respectively; torsional damping above and below the regulator: with damping coefficients D_{Φ_a} and D_{Φ_b}, respectively), the stiffness (the torsional stiffness of long drill-pipes C_p and the stiffness of the regulator K_b), gravitational forces (from the total masses above and below the regulator: M_a and M_b, respectively), and the top-side boundary conditions (the hookload H_0 and angular velocity Ω_0 imposed at surface). The WOB and TOB due to the cutting process in the bit-rock interaction are also included in this column $\mathbf{h}$ in Eq. (1). For the torsional dynamics, two inertias of the drillstring components are considered: 1) I_a for the upper part – above the regulator, and 2) I_b for the lower part – below the regulator.

The generalized displacement coordinates of this drilling system model in Eq. (1) are given by

$$\mathbf{q} = \begin{bmatrix} U & U_b & \Phi_b \end{bmatrix}^{\mathrm{T}}, \tag{2}$$

where the axial displacement of the lumped drillstring section above the regulator (as the upper part) is denoted by U. The generalized coordinates for describing the drillstring response at the bit (as the lower part) are the axial and angular displacements of the drill bit, respectively denoted as U_b and Φ_b. Note that due to a kinematic constraint induced by the design of the downhole regulator (i.e., the helical spline denoted by h_b in Figure 6), we can eliminate one of the original coordinates of the lumped model in Figure 6. Please refer to (T. Vromen et al., 2019; Wildemans et al., 2019) for further detail derivations.

The contact force and the frictional torque acting on the bit and the frictional forces and torques acting on the stabilizers in Eq. (1) are collected in the column vector $\boldsymbol{\lambda}$ that is composed by:

$$\boldsymbol{\lambda} = \begin{bmatrix} \lambda_{b_a} & \lambda_{b_t} & \lambda_{T_a} & \lambda_{T_t} & \lambda_{T_{ba}} & \lambda_{T_{bt}} \end{bmatrix}^{\mathrm{T}}, \tag{3}$$

The frictional force and torque acting above the regulator (i.e., on the upper stabilizer; see Figure 5) are lumped into λ_{T_a} and λ_{T_t}, respectively. The frictional force and torque acting below the regulator (i.e., on the lower stabilizer; see Figure 5) are lumped into $\lambda_{T_{ba}}$ and $\lambda_{T_{bt}}$, respectively. Moreover, the contact force and frictional torque due to the bit-rock interaction are represented by $\lambda_{b_a} = -W^f$ and $\lambda_{b_t} = -T^f$, respectively. These weight W^f and torque T^f are calculated via the frictional component of the bit-rock interface laws. The matrix $\boldsymbol{W}_\lambda$ in Eq. (1) denotes the generalized directions of these frictional and contact force/torque components.

In this model, the spatial friction is considered acting partly above and partly below the regulator as shown in Figure 5. Thus, the associated normal force (F_N) is distributed between the two locations, namely above (ΔF_N) and below the regulator ($(1\text{-}\Delta)F_N$); see Figure 5. As introduced above, the frictional forces and torques at the stabilizers above and below the regulator are given by $\boldsymbol{\lambda}_T = \begin{bmatrix} \lambda_{T_a} & \lambda_{T_t} \end{bmatrix}$ and $\boldsymbol{\lambda}_{T_b} = \begin{bmatrix} \lambda_{T_{ba}} & \lambda_{T_{bt}} \end{bmatrix}$, respectively. The subscripts a and t denote for the two spatial directions of the friction, respectively, axial and tangential (see the red arrows in Figure 6). In addition, the admissible friction forces above and below the tool are, respectively, formulated by the following convex sets (Wildemans, 2018):

$$C_T = \left\{ \boldsymbol{\lambda}_T \in \boldsymbol{R}^2 \middle| \| \boldsymbol{\lambda}_T \| \leq \mu_w F_N \right\}, \qquad C_{T_b} = \left\{ \boldsymbol{\lambda}_{T_b} \in \boldsymbol{R}^2 \middle| \| \boldsymbol{\lambda}_{T_b} \| \leq (1-\Delta)\mu_w F_N \right\}, \tag{4}$$

with μ_w as the friction coefficient for these contacts. The range of the distribution parameter is considered as follows: $\Delta \in [0,1]$, where the spatial friction only acts above the regulator when $\Delta = 1$ holds. Otherwise, the spatial friction only acts below the regulator when $\Delta = 0$ holds. The normal force in Eq. (4) is defined as follows:

$$F_N = B_f M_{ds} g \sin\Theta, \tag{5}$$

where B_f denotes the buoyancy factor of the mud (for the submerged part of the drillstring), M_{ds} is the mass of the drillstring, g is the gravitational acceleration, and Θ is the inclination angle of the wellbore).

The total force and torque acting on the drill-bit from the bit-rock interface laws (as the combination of the friction and cutting process of the bit-rock interaction) can be summarized, respectively, as follows:

$$W = W^c + W^f; \quad T = T^c + T^f, \tag{6}$$

with W^c and T^c denoting for the WOB and TOB of the cutting component, respectively. These total WOB W and total TOB T in Eq. (6) are dependent on the bit and rock parameters associated to the cutting and frictional components, which are assumed to be homogeneous in this scenario.

The WOB and TOB of the cutting component are given, respectively, by (Detournay & Defourny, 1992; Detournay *et al.*, 2008)

$$W^c = na\varepsilon\varsigma d_n, \text{ and } T^c = \frac{1}{2}na^2\varepsilon d_n, \tag{7}$$

with the parameter ε denoting the intrinsic specific energy of the rock, the bit radius a, the number of (identical) bit blades n, and the constant ς representing the inclination of the cutting force (affected by the bit profile/shape). The depth-of-cut (DOC) d_n produced via the rock cutting process is calculated based on the bit axial displacement as follows:

$$d_n = U_b(t) - U_b(t - t_n), \tag{8}$$

with t denoting the current time and t_n the time delay due to the regenerative effect in the cutting process. This time delay is calculated via the *implicit* delay equation of the bit angular displacement as follows:

$$\Phi_b(t) - \Phi_b(t - t_n) = \frac{2\pi}{n}. \tag{9}$$

The WOB and TOB of the frictional component are given, respectively, by the following set-valued force laws:

$$W^f \in na\sigma l_n \frac{1 + \mathrm{Sign}(V_b)}{2}, \quad \text{and } T^f \in \frac{n}{2}a^2\mu\sigma l_n\xi\mathrm{Sign}(\Omega_b). \tag{10}$$

These frictional components are parameterized by: 1) the maximum contact pressure σ at the cutter wearflat, 2) the coefficient of friction μ (at the contact between the wearflat and rock), 3) the wearflat length l_n describing the cutter bluntness, and 4) the constant ξ representing the orientation of the contact force on the wearflat (also affected by the bit profile). The bit axial and angular velocities are denoted by $V_b = \dot{U}_b$ and $\Omega_b = \dot{\Phi}_b$, respectively.

Note that the inclusions in Eq. (10) indicate the non-smooth nature of the contact and friction laws at the bit-rock interface, which will require a specific treatment in the numerical computations. To study the effect of the downhole regulator on drilling performance, the dynamic responses of the drillstring with DR are required, which can be obtained via a computational algorithm for numerically solving the governing equations in Eq. (1) as detailed in (Wildemans, 2018; Wildemans et al., 2019).

Dynamic model of drilling system with downhole regulator in interbedded formations

The overview of the drilling system equipped with a downhole regulator in interbedded formation is depicted in Figure 7 (Aribowo *et al.*, 2022b). The interbedded formation considered here consists of layers with two distinct rock properties, namely soft (in green) and hard (in red) rock layers. The same downhole regulator design as in the previous scenario is also considered here.

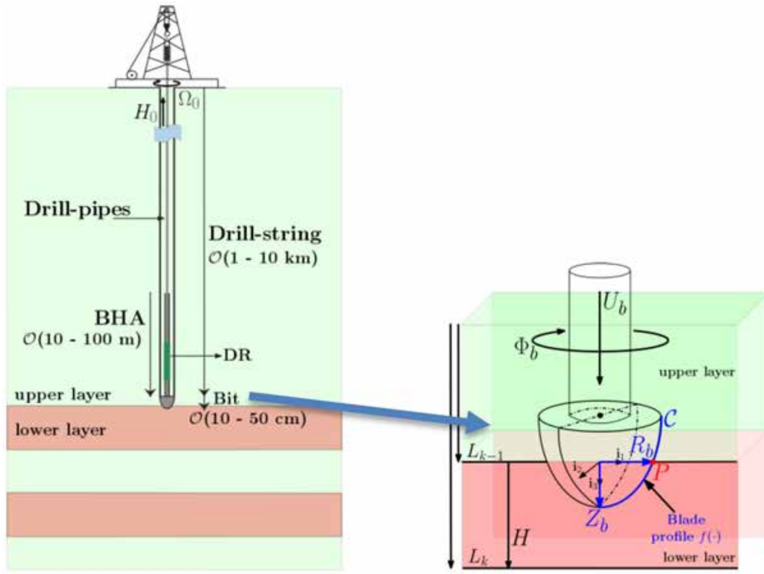

Figure 7—Schematic overview of rotary drilling system equipped with DR in a vertical well-bore during a transitional phase between two rock layers – see (Aribowo et al., 2022b).

A lumped-parameter model in Figure 8, which is also similar to the one used in the previous scenario, is used to construct the EOMs of this drilling system in interbedded formations. The difference between the model in Figure 8 and that in Figure 6 is only related to two aspects. Firstly, the bit-rock interaction changes in the scenario with an interbedded formation involving layer transitions. Secondly, in the latter scenario we consider vertical drilling and the effect of deviated wellbore is omitted (no spatial Coulomb friction between stabilizers and borehole wall). The top boundary conditions are the same as in the previous scenario.

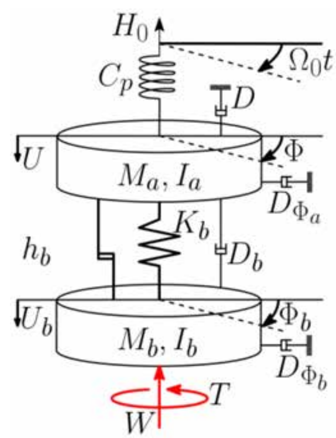

Figure 8—Lumped-parameter model of drillstring system equipped with DR (DR model) and affected by the bit-rock interaction in interbedded formations - see (Aribowo et al., 2022b).

The bit-rock interface laws for interbedded formations developed in (Aribowo *et al.*, 2022a) are employed as the bottom boundary conditions in this drilling scenario, which considers a transitional phase of the bit motion in two distinct horizontal rock layers as depicted in Figure 7 (right side). The interface laws in (Aribowo *et al.*, 2022a) extend the interface laws earlier developed in (Detournay & Defourny, 1992; Detournay *et al.*, 2008) in order to capture the contributions of the interaction between the drill-bit and the associated rock layer(s) to the forces and torques acting on the bit (WOB and TOB) during the transitional phase. This change in the characteristics of the bit-rock interface laws in turn affects the drilling system dynamics. These interface laws are applied for the scenario of involving multiple layer transitions of the bit motion when drilling interbedded formation.

In order to calculate the contributions of the interaction of the lower and upper parts of the bit with the associated rock layer(s) in which the bit is currently engaged, the bit engagement parameter Z_b is introduced as an evolution parameter. This parameter is used to determine which part of the bit is engaged in the upper and lower rock layers in a transitional phase (see the illustration in the right side of Figure 7). As the bit progresses into the lower layer, this engagement parameter is updated based on the bit axial displacement U_b and (a priori known) geological layer structure of the formation.

By using the current value of this evolution parameter, the bit-rock parameters (of the associated layer(s)) for the cutting and frictional components of the interface laws are updated in order to calculate the current values of WOB and TOB. The update on the bit parameters can be done by also taking advantage of the following mapping (based on the system of coordinates on the bit):

$$z_b = f(r_b), \tag{11}$$

where z_b and r_b are the dimensionless values of the bit engagement Z_b and the bit radius at the layer interface R_b, respectively. The dimensionless function $f(\bullet)$ denotes the bit profile (shape) function; see Figure 7. In this way, the effect of bit design (represented by this profile function f) on the total dynamics of the drilling system can be also implicitly included.

In a quite similar form of the EOMs in Eq. (1), the governing equations for the axial and torsional dynamics of this drilling system with the downhole regulator in interbedded formation are written in the following form:

$$\overline{\mathbf{M}}\ddot{\mathbf{q}} - \overline{\mathbf{h}}(t, \mathbf{q}, \dot{\mathbf{q}}) = \mathbf{S}[W \quad T]^{\mathrm{T}}, \tag{12}$$

where $\overline{\mathbf{M}}$ is the mass matrix and the column vector $\overline{\mathbf{h}}$ contains all generalized (smooth) forces and torques, which excludes the contact forces and the frictional torques acting on the bit. The generalized coordinates $\mathbf{q}$ for describing the model response in this scenario are considered the same as in Eq. (2). The difference is that the cutting and frictional components of the bit-rock interface laws (in terms of total WOB W and total TOB T) are written in the right-hand-side (RHS) of Eq. (12). The matrix S denotes the generalized force directions related to the interface laws.

Based on (Aribowo *et al.*, 2022a) and following Eq. (6), these total weight and torque acting on the drill-bit due to the bit-rock interaction with a transitional phase involving two different rock layers are given, respectively, by

$$W = \left(W^c_{k-1} + W^c_k\right) + \left(W^f_{k-1} + W^f_k\right), \tag{13}$$

and

$$T = \left(T^c_{k-1} + T^c_k\right) + \left(T^f_{k-1} + T^f_k\right). \tag{14}$$

The subscript $k-1$ denotes for the upper rock layer, and the subscript k is for the lower rock layer. These components of total WOB and total TOB are calculated for each upper and lower layer based on the bit-rock parameters of the associated layers (i.e., as the extended versions of Eq. (7) and Eq. (10)). The involved parameters are updated along the bit progression in the lower layer via the bit engagement Z_b. For the cutting component, the total WOB and TOB of the upper and lower layers are given, respectively, by

$$W^c_{k-1} + W^c_k = na\zeta^* d_n\left(\varepsilon_{k-1}\left(1 - \vartheta^{\zeta}_k\right) + \varepsilon_k \vartheta^{\zeta}_k\right), \tag{15}$$

and

$$T^c_{k-1} + T^c_k = \frac{a^2}{2} n d_n\left(\varepsilon_{k-1}\left(1 - r^2_b\right) + \varepsilon_k r^2_b\right). \tag{16}$$

The bit parameters ζ^* and ϑ_k^{ζ} are related to the inclination of the cutting force in the associated layer(s) and updated by the bit engagement Z_b (via the bit profile/shape function), see (Aribowo *et al.*, 2022a). For the frictional component, the total WOB and TOB of the upper and lower layers are given, respectively, by

$$W_{k-1}^f + W_k^f \in \left(\sigma_{k-1}\left(1-r_b\right)+\sigma_k r_b\right) na\ell_n \frac{1+\mathrm{Sign}\left(V_b\right)}{2}, \tag{17}$$

and

$$T_{k-1}^f + T_k^f \in \frac{\left(\mu_{k-1}\sigma_{k-1}(1-\vartheta_k^{\xi}) + \mu_k\sigma_k\vartheta_k^{\xi}\right)a\xi\left(W_{k-1}^f + W_k^f\right)}{2\left(\sigma_{k-1}\left(1-r_b\right)+\sigma_k r_b\right)} \mathrm{Sign}\left(\Omega_b\right). \tag{18}$$

The bit parameter ϑ_k^{ξ} is related to the orientation of the contact force on the wearflat in the associated layer(s) and also updated by the bit engagement Z_b (via the bit profile/shape function), see (Aribowo *et al.*, 2022a).

The dynamic response of this model of the drillstring with a downhole regulator in this interbedded formation scenario in Eq. (12) can be obtained via a similar computational algorithm for numerically solving the governing equations in Eq. (1) as detailed in (Aribowo *et al.*, 2022b).

Simulation results for deviated and interbedded scenarios

In this section, we summarize the simulation results and the associated analyses for the dynamic models of a drilling system with the downhole regulator presented in the previous section. This summary provides the illustrations for each drilling scenario on how the use of such downhole regulator affects drilling performance in terms of (averaged) ROP and drilling efficiency. The response of a dynamic model without the downhole regulator will be denoted as the benchmark model (BM) model response[1], while the response of the dynamic model with the regulator will be denoted as the downhole-regulator (DR) model response.

Deviated well scenario

The simulation results for this deviated wellbore scenario are based on the results presented in (Wildemans et al., 2019). Figure 9 and Figure 10 show the plots of averaged ROP and drilling efficiency for the cases of deviated wellbore with an inclination angle $\Theta = 45°$ and vertical wellbore ($\Theta = 0°$ no spatial contact above and below the regulator), respectively, for both the BM and the DR models. These simulations are run for a hookload varying in the range of H_0 = 370-440 kN with a constant top angular velocity Ω_0 = 80 RPM.

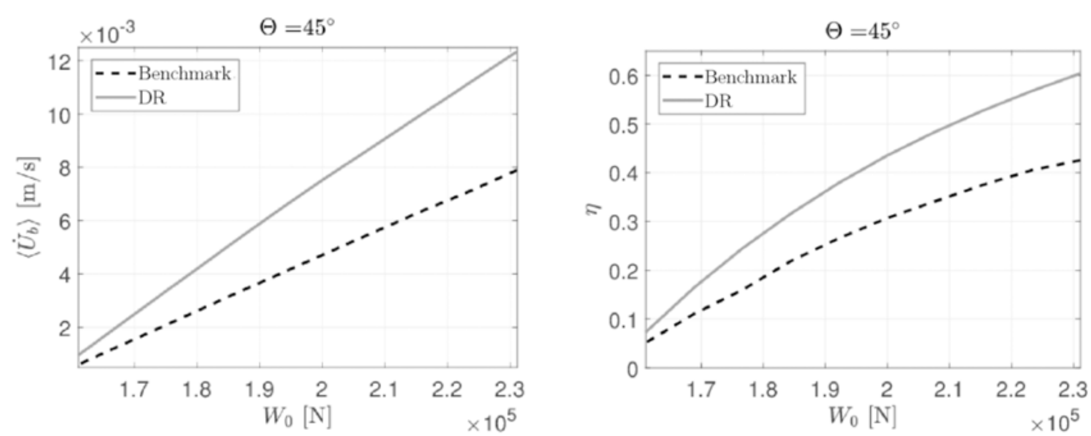

Figure 9—Comparison of the BM model and the DR model in terms of averaged ROP (left) and drilling efficiency (right) in a deviated well (with inclination angle $\Theta = 45°$) under the variation of applied WOB at the top – see (Wildemans et al., 2019).

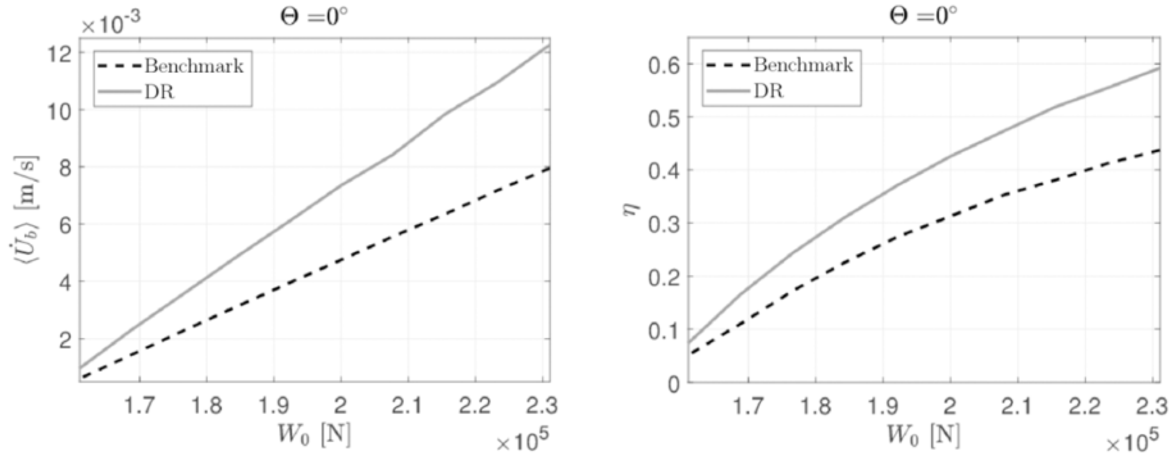

Figure 10—Comparison of the BM model and the DR model in terms of averaged ROP (left) and drilling efficiency (right) in a vertical well (with inclination angle $\Theta = 0 = 45°$) under the variation of applied WOB at the top – see (Wildemans et al., 2019).

Note that in both plots the applied (nominal) weight W_0 at the top is used for the horizontal axis (instead of using the hookload values directly), and this weight is given by

$$W_0 = W_s - H_0 \tag{19}$$

with W_s denoting the submerged weight of the drillstring (in the drilling mud). The drilling efficiency for the cutting process is calculated based on the ratio between the averaged value of TOB due to the cutting and the sum of the averaged values of TOB in both (cutting and frictional) components of the interface laws:

$$\eta = \frac{\langle T^c \rangle}{\langle T^c \rangle + \langle T^f \rangle} \tag{20}$$

with the bracket $\langle \bullet \rangle$ denoting for the averaged value of the associated response.

From Figure 9, we see that in a deviated wellbore scenario the averaged ROP and the efficiency in the DR model (grey-solid line) are higher than the ones in the BM model (black-dashed line), and also increase with the applied weight W_0. These findings indicate the positive effect of the regulator on these two performance quantities, which are also comparable as observed in the case of vertical wellbore in Figure 10. Some cases with different inclination angle reported in (Wildemans, 2018; Wildemans et al., 2019) also reveal the same tendencies for the effect of the regulator on drilling performance.

The physical reasoning supporting behind this effect of the regulator in a case of deviated wellbore follows the explanation detailed in (T. Vromen *et al.*, 2019) where the contraction of the regulator helps in two ways, namely 1) to reduce the frictional loading on the drill-bit (i.e., due to the contact at the wearflat interface), and, 2) as a consequence, to increase weight and torque on bit related to the cutting process (i.e., which in fact leads to bit progression and ROP). This reasoning will be more detailed later when presenting the simulation results in the case of interbedded formation.

Interbedded formation scenario

The simulation results for this interbedded formation scenario based on (Aribowo *et al.*, 2022b) are summarized here to illustrate the effect of the downhole regulator on drilling performance under such case. For this purpose, this case study considers an interbedded formation composed by soft (in green) and hard (in red) rock layers with a periodic sequence of soft-hard layer structure. The rock parameters of these two layers (associated to the components of the interface laws) are listed in Table 1.

Table 1—Rock parameters for soft and hard layers.

Parameter Name	Soft Layer	Hard Layer	Unit
Intrinsic specific energy (ε)	150	200	Mpa
Contact pressure (σ)	150	200	Mpa
Friction coefficient (μ)	0.75	1.0	[-]
Bit height (b)	22.2	22.2	Cm

Moreover, thin layers in terms of the ratio *H/b#{1,2,…,10}* between the layer thickness H and bit height b are also considered. The thickness of each layer is considered to be the same. For the drilling operations parameters imposed at surface, we apply two hookload values (corresponding to higher and lower applied weights) and a constant top angular velocity Ω_0 = 80 RPM.

Figure 11 shows the response of bit axial velocities (ROP) of the DR model in interbedded formation with the thickness of each layer the same as the bit height ($H = b$) and the hookload $H_0 = 440\ kN$. The black vertical lines between these green (soft layer) and red (hard layer) areas indicate the time when the bit starts to progress into the lower (new) layer.

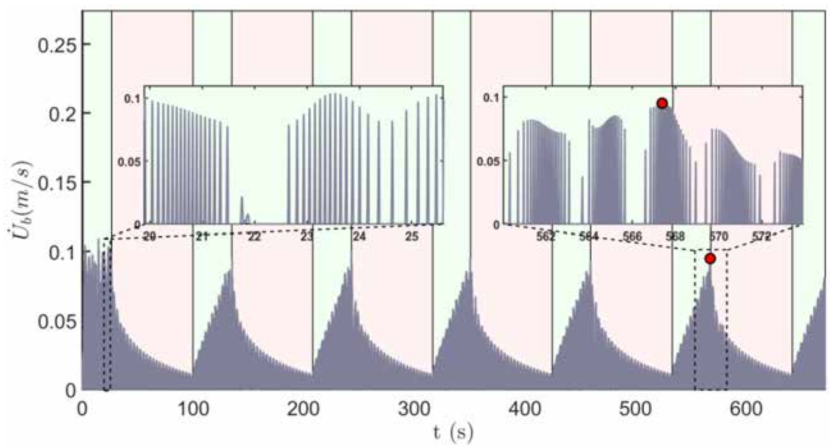

Figure 11—Axial dynamic (bit axial velocity) response of the drillstring with downhole regulator (DR) model in interbedded formation (layer thickness $H = b$) – see (Aribowo et al., 2022b)

The plot located in the first green area in Figure 11 (i.e., the left-zoomed plot) shows the dynamic response in the homogeneous soft layer, while the right-zoomed plot in Figure 11 shows the dynamic response during a transitional phase of the bit motion from soft (green) to hard (red) layers. Due to the limited thickness of the layers ($H = b$), the dynamic responses in the right-zoomed plot do not have sufficient time to converge to the steady-state responses associated with a homogeneous (either hard or soft) layer. Hence, the comparison between the right- and left-zoomed plots in Figure 11 indicates that the response in the case of interbedded formation is essentially different from that in homogeneous formation. Moreover, as expected, the ROP increases in soft (green) layer and decreases in hard (red) layer. Hence, due to the same thickness of each layer, the time duration in soft layer is significantly shorter than in the hard layer.

Calculation of the averaged value of the steady-state responses in interbedded formation is detailed in (Aribowo *et al.*, 2022b; Aribowo *et al.*, 2022c), and we utilize this averaged value for analyzing the effect of the regulator on drilling performance in interbedded formation. The averaged value of ROP in interbedded formations reads as follows (Aribowo *et al.*, 2022c, 2022b):

$$\langle \dot{U}_b \rangle = \frac{2\langle \dot{U}^b_{k-1}\rangle\langle \dot{U}^b_k\rangle}{\langle \dot{U}^b_{k-1}\rangle + \langle \dot{U}^b_k\rangle}. \tag{21}$$

Note that $\langle \dot{U}^{b}_{k-1} \rangle$ and $\langle \dot{U}^{b}_{k} \rangle$ are the averaged ROP in each upper and lower layer, respectively. Moreover, the drilling efficiency in each layer is given by:

$$\eta_k = \frac{\langle T^{c}_{k} \rangle}{\langle T^{c}_{k} \rangle + \langle T^{f}_{k} \rangle}. \tag{22}$$

By utilizing Eq. (22) and the averaging formulation introduced in (Aribowo *et al.*, 2022b, 2022c), the averaged value of drilling efficiency in interbedded formation (upper and lower layers) is calculated as follows:

$$\eta = \left(1 + \frac{\eta_{k-1} \langle \dot{U}^{b}_{k} \rangle}{\eta_k \langle \dot{U}^{b}_{k-1} \rangle} \right) \frac{\eta_k \langle \dot{U}_b \rangle}{2 \langle \dot{U}^{b}_{k} \rangle}. \tag{23}$$

Figure 12 and Figure 13 compare the BM (solid line) and the DR model (dashed line) in terms of the averaged ROP $\langle \dot{U}_b \rangle$ and the averaged drilling efficiency η, respectively, in interbedded formation case with each varied layer thickness (in terms of the ratio $H/b\#\{1,2,\dots,10\}$). The comparisons are done for two different hookload values H_0 $\#\{420,440\}kN$ (in red and blue lines, respectively).

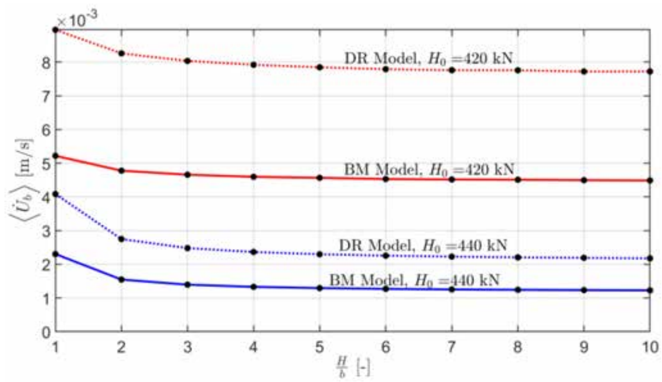

Figure 12—The comparison of the averaged ROP between the drilling system models without and with the downhole regulator (BM model in solid line and DR model in dashed line, respectively) under the effects of the layer thickness variation ($H/b\#\{1,2,\dots,10\}$), for two hook-load values $H_0 = 440$ kN (blue) and $H_0 = 420$ kN (red) with top angular velocity $\Omega_0 = 80$ RPM – see (Aribowo et al., 2022b).

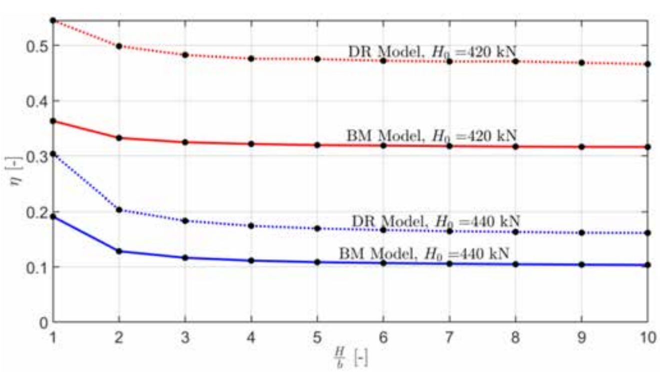

Figure 13—The comparison of the drilling efficiencies between the drilling system models without and with the downhole regulator (BM model in solid line and DR model in dashed line, respectively) under the effects of the layer thickness variation ($H/b\#\{1,2,\dots,10\}$), for two hook-load values $H_0 = 440$ kN (blue) and $H_0 = 420$ kN (red) with top angular velocity $\Omega_0 = 80$ RPM – see (Aribowo et al., 2022b).

These comparisons in Figure 12 and Figure 13 show that the use of such downhole regulator improves significantly the ROP and the efficiency (almost double in average) under such variation of layer thickness in drilling interbedded formation. A consistent increasing tendency of these two performance quantities in DR model is also observed with the change of the imposed hookload.

In order to detail the mechanisms by which this regulator enables the increase in drilling performance for such drilling scenario, we analyze the averaged cutting force ratio $\bar{\mathcal{W}}^c$ and averaged wearflat contact force ratio $\bar{\mathcal{W}}^f$ as formulated in (Aribowo *et al.*, 2022c, 2022b). Note that the average values of the cutting force ratio and the contact force ratio in each layer are given, respectively, by

$$\bar{\mathcal{W}}_k^c = \frac{\langle W_k^c \rangle}{\langle W_k^c \rangle + \langle W_k^f \rangle}, \text{ and } \quad \bar{\mathcal{W}}_k^f = \frac{\langle W_k^f \rangle}{\langle W_k^c \rangle + \langle W_k^f \rangle}. \tag{24}$$

Let us refer to Figure 14 and Figure 15 that show the plots of averaged cutting force ratio and averaged wearflat contact force ratio, respectively, for both BM and DR models under the same drilling cases. In Figure 14, we observe the increase of averaged cutting force ratio in DR model to this ratio in BM model (with consistent tendencies for each associated hookload). Moreover, we discover the reverse effect in the averaged contact force ratio in Figure 15 where this ratio tends to decrease in DR model response compared to the one in BM model.

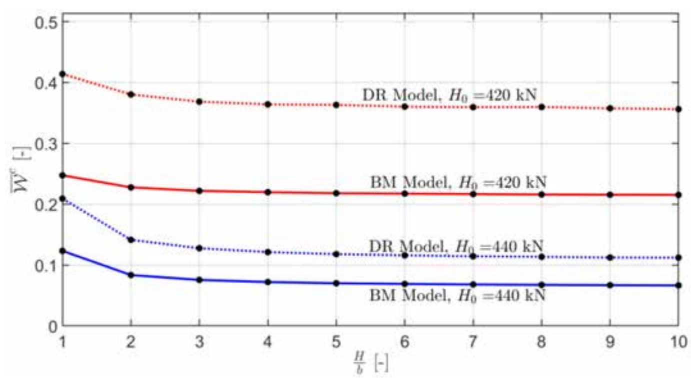

Figure 14—The comparison of the (averaged) cutting force ratio between the drilling system models without and with the downhole regulator (BM model in solid line and DR model in dashed line, respectively) under the effects of the layer thickness variation (*H/b#{1,2,…,10}*), for two hook-load values $H_0 = 440$ kN (blue) and $H_0 = 420$ kN (red) with top angular velocity $\Omega_0 = 80$ RPM – see (Aribowo et al., 2022b).

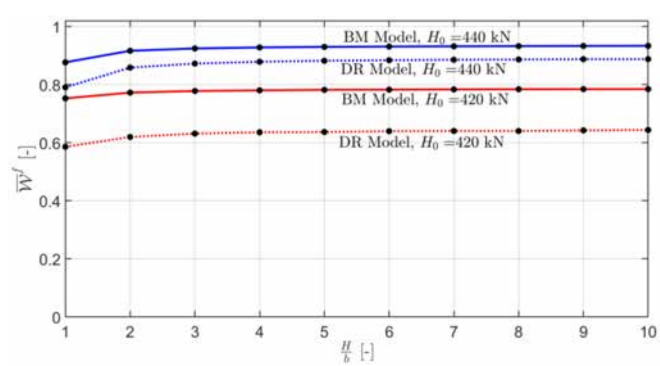

Figure 15—The comparison of the (averaged) wear-flat contact force ratio between the drilling system models without and with the downhole regulator (BM model in solid line and DR model in dashed line, respectively) under the effects of the layer thickness variation (*H/b#{1,2,…,10}*), for two hook-load values $H_0 = 440$ kN (blue) and $H_0 = 420$ kN (red) with top angular velocity $\Omega_0 = 80$ RPM – see (Aribowo et al., 2022b).

Thus, this model-based results show the mechanism that supports the use of regulator in assisting to improved drilling efficiency. In addition, the latter observation indicates that the use of regulator can lower the frictional losses in the bit-rock interaction (i.e., via the contraction of the regulator). Equivalently, this also shows less frictional loading on the bit and more weight used for the cutting in the DR model (all in averaged sense); these are the same findings as those obtained by (Vromen *et al*., 2019) for a different drilling case.

As a final remark from the comparison between the simulation results of the theoretical models for each drilling scenario and the field data statistics, we obtain qualitatively consistent indications on the performance improvement with the application of DR in the drillstring.

Firstly, the DR leads to higher ROP in a broad range of scenarios. Secondly, the DR leads to reduced frictional losses at the bit, which may consequently decrease the (averaged) temperature at the PDC cutters. We note that both elevated temperature and contact force are drivers for bit wear, i.e., a high temperature, beyond over a certain limit, weakens the bindings in the polycrystalline diamond structure. This undesired effect can cause fragments of the diamond to be more easily ripped out. In the field statistical data, the durability of the bit can potentially be related to drilling distance per run or footage. A further study for taking into account the effect of the higher-order dynamic modes of the drillstring dynamics (i.e., the distributed behavior of long-slender drillstring structure) on the working performance of such downhole regulator shall be considered as the next modeling step, in order to check the consistency of the comparison results.

Conclusion

In this paper, we present the field data statistics describing the effect of downhole regulator application on drilling performance (in terms of ROP and footage gains) for drilling in the offshore fields of Equinor. We also summarize the developed theoretical models of drilling systems equipped with a downhole regulator for two separated scenarios, namely drilling in deviated wellbore and drilling in interbedded formations.

From the numerical simulations, the effect of such downhole regulator on drilling performance is studied under the influence of these drilling scenarios, separately. The simulation-based findings suggest that the use of such downhole regulator can be a mechanism in the drillstring that will assist for autonomously managing the dynamic loadings on the bit and gaining the increase on drilling performance in terms of (averaged) ROP and drilling efficiency.

From the comparison between the theoretical and field results, the simulation-based findings show how the gain in drilling performance qualitatively aligns with the statistical results from using a full-scale version of the downhole regulator in Equinor operations.

Acknowledgments

This study is also supported by the Indonesian Endowment Fund for Education (LPDP) of the Republic of Indonesia (Grant No. PRJ-4653/LPDP.3/2016).

The authors want to acknowledge Equinor for their role in the development, field deployment and documentation of the DR technology.

References

Aribowo, A. G., Wildemans, R., Detournay, E., & van de Wouw, N. (2022a). Drag bit/rock interface laws for the transition between two layers. *International Journal of Rock Mechanics and Mining Sciences*, **150**, 104980. https://doi.org/10.1016/j.ijrmms.2021.104980

Aribowo, A. G., Wildemans, R., Detournay, E., & van de Wouw, N. (2022b). Dynamic Analysis of a Down-Hole Regulator (AST) for Drilling in Interbedded Formations. Submitted to SPEJ.

Aribowo, A. G., Wildemans, R., Detournay, E., & van de Wouw, N. (2022c). Dynamic Modeling of Drill-String Systems for Layered Rock Formations. In 5th International Colloquium on Nonlinear Dynamics and Control of Deep Drilling Systems, UMD, College Park, MD, U.S.A., 2022. College Park, MD, U.S.A. https://doi.org/https://doi.org/10.1007/s11071-019-05075-6

Beeh, H. A., Khalil, H., Paulus, S. L., Tiku, A., & Karlsen, B. A. (2018). Thorough analysis and commitment for improvement led to a step change in the drilling performance on valemon field, north sea. In Society of Petroleum Engineers - *SPE Norway One Day Seminar 2018* pp. 230–244. https://doi.org/10.2118/191316-ms

Detournay, E., & Defourny, P. (1992). A phenomenological model for the drilling action of drag bits. *International Journal of Rock Mechanics and Mining Sciences and Geomechanics Abstracts*, **29**(1), 13–23.

Detournay, E., Richard, T., & Shepherd, M. (2008). Drilling response of drag bits: theory and experiment. *International Journal of Rock Mechanics and Mining Sciences*, **45**(8), 1347–1360.

Fear, M. J., Abbassian, F., Parfitt, S. H. L., & McClean, A. (1997). The Destruction of PDC Bits by Severe Slip-Stick Vibration. In SPE/IADC Drilling Conference, Amsterdam, 4 – 6 March 1997. Amsterdam, Netherlands. https://doi.org/10.2118/37639-MS

Johancsik, C. A., Friesen, D. B., & Dawson, R. (1984). Torque and Drag in Directional Wells - Prediction and Measurement. *JPT, Journal of Petroleum Technology*, **36**(7), 987–992. https://doi.org/10.2118/11380-pa

Leine, R. I., & van de Wouw, N. (2008). Stability and Convergence of Mechanical Systems with Unilateral Constraints. (Pfeiffer F. & Wriggers P., Eds.) (Vol. **36**). Berlin, Heidelberg: Springer-Verlag.

Selnes, K. S., Clemmensen, C., & Reimers, N. (2008). Drilling Difficult Formations Efficiently with the Use of an Antistall Tool. In Proceedings of IADC/SPE Drilling Conference in Orlando, Florida, USA, 4 - 6 March 2008 pp. 531–536. https://doi.org/10.2118/111874-MS

Selnes, K. S., Clemmensen, C., & Reimers, N. (2009). Drilling Difficult Formations Efficiently with the Use of an Antistall Tool. *SPE Drilling and Completion*, **24**(04), 531–536. https://doi.org/https://doi.org/10.2118/111874-PA

Sheppard, M. C., Wick, C., & Burgess, T. (1987). Designing Well Paths To Reduce Drag and Torque. *SPE Drilling Engineering*, **2**(04), 344–350. https://doi.org/10.2118/15463-PA

Vromen, T., Detournay, E., Nijmeijer, H., & van de Wouw, N. (2019). Dynamics of drilling systems with an antistall tool: effect on rate of penetration and mechanical specific energy. *SPE Journal*, **24**(05), 527. https://doi.org/https://doi.org/10.2118/194487-PA

Vromen, T. G. M. (2015). Control of stick-slip vibrations in drilling systems. Eindhoven Univeirsity of Technology, PhD Thesis.

Wildemans, R. (2018). Modelling and dynamic analysis of an anti-stall tool in a drilling system including spatial friction. Eindhoven Univeirsity of Technology, MSc Thesis.

Wildemans, R., Aribowo, A., Detournay, E., & van de Wouw, N. (2019). Modelling and dynamic analysis of an anti-stall tool in a drilling system including spatial friction. *Nonlinear Dynamics*. https://doi.org/10.1007/s11071-019-05075-6